58918-00-105

CONF-900577--2

MAGNETIC PROPERTIES OF ULTRATHIN EPITAXIAL FILMS OF IRON*

INVITED

CONF-900577--2

DE90 017861

C. Liu and S. D. Bader

Materials Science Division

Argonne National Laboratory, Argonne, IL 60439, USA

Invited paper for the European Materials Research Society (E-MRS) 1990 Spring Meeting, Strasbourg, France, May 29-June 1, 1990. **Symposium C: Magnetic Thin Films, Multilayers and Superlattices.** Proc. to be published as a special issue of Journal of Magnetism and Magnetic Materials.

jmc

*Work supported by U.S. Department of Energy, BES-Materials Sciences contract #W-31-109-ENG-38.

MAGNETIC PROPERTIES OF ULTRATHIN EPITAXIAL FILMS OF IRON

C. Liu and S. D. Bader

Materials Science Division

Argonne National Laboratory, Argonne, Illinois 60439 USA

ABSTRACT

Ultrathin Fe films epitaxially grown on Cu(100), Au(100), Pd(100), and Ru(0001) substrates are used to study monolayer magnetism, surface magnetic anisotropy and two-dimensional (2D) critical behavior, by means of *in-situ* surface magneto-optical Kerr-effect measurements. Epitaxial structures and growth modes are characterized by auxiliary low-energy electron diffraction and Auger electron studies. The magnetic properties of the films depend on the growth temperature. For 100-K growth, all films exhibit a universal behavior of perpendicular spin orientations in the monolayer regime, while for 300-K growth, Fe/Pd(100) and Fe/Au(100) have in-plane easy-axis of magnetization for all thicknesses. Fe/Ru(0001) lacks a ferromagnetic response for thicknesses less than two monolayers (ML). Fe/Pd(100) has remarkable thermal stability in the monolayer and submonolayer range. Reversible magnetization data are obtained for 0.6 to 3.0-ML-thick films, which show second-order phase transitions at thickness-dependent Curie temperatures (T_C). An effective magnetization exponent β_{eff} of 0.127 ± 0.004 is obtained for a 1.2-ML Fe/Pd(100) film, in agreement with the theoretical value of $\beta_c = 0.125$ for an ideal 2D Ising model. The T_C trend with film thickness for Fe/Pd(100) is also in agreement with Monte-Carlo calculations for Ising films.

1. INTRODUCTION

For over 40 years there has been interest in two-dimensional (2D) phase transitions and 2D critical behavior. Onsager's solution [1] for an ideal 2D Ising model is a landmark achievement of theoretical physics. It represents one of the few solutions to physical problems that can be solved analytically. The order parameter of a 2D Ising system follows a power-law behavior [2,3] as the transition temperature T_C is approached, and is characterized by a critical exponent $\beta_c = 1/8$. In contrast, it has been shown exactly [4] that for a 2D isotropic Heisenberg system there is no long-range order at finite temperature. For more complicated systems approximations and numerical methods are widely used [5,6]. An important conclusion derived from Monte-Carlo calculations is that a 2D Heisenberg system with anisotropy will have Ising-like behavior [7,8]. The theoretical conclusions need clear experimental confirmations for magnetic systems. In early work, for example, an effective exponent β_{eff} of 0.56 was reported for Ni films (260-1340 Å thick) grown on mica [9]. This β_{eff}-value lies between the predicted 3D value [10] of 0.38 and the surface value [11] of 0.8. For films to serve as physical realizations of 2D Ising systems, they must be much thinner than the lateral correlation length, which is limited by the ~10^2-Å size of the flat substrate terrace regions. This requires experiments in the monolayer regime. Also clean and well-ordered films are needed. It is only quite recently that such systems have become available [12-14]. Dürr, *et al.* [12] studied Fe/Au(100) and extracted an effective exponent β_{eff} of 0.22. This β-value deviates from the theoretical value of 1/8 and raises many questions.

The present work explores the monolayer regime using the system Fe/Pd(100). It is well known from Fe dilute-alloy studies [15, 16] that Fe atoms in a Pd host polarize the surrounding Pd atoms, resulting in giant magnetic moments. Fe overlayers on a Pd substrate also polarize the top Pd layers, as calculated theoretically [17]. We find that Fe/Pd(100) exhibits monolayer and even submonolayer ferromagnetism. Moreover, it has remarkable thermal stability and reversibility in the

monolayer range. It also possesses the perpendicular surface magnetic anisotropy in the monolayer region which supports an Ising-like description of the phase transition.

Perpendicular spin orientations in the ultrathin limit [18, 19] have been confirmed in our laboratory for Fe/Cu(100) [20, 21], Fe/Au(100) [22], Fe/Ru(0001) [23] and Fe/Pd(100) [22] films. The complex interfacial morphology and the Fe-substrate electronic interactions make the experimental characterizations quite challenging. Previous work on Fe/Au(100) [12, 24] failed to detect perpendicular easy axes of magnetization because reduced growth temperatures are needed to suppress interfacial mixing. For metal-on-metal systems, electronic hybridization between the overlayer and the substrate atoms plays a crucial role in determining the magnetic properties of the system. Hybridization destroys the ferromagnetism of the first two layers of Fe/Ru(0001), while it induces moments on the interfacial Pd in Fe/Pd(100), as mentioned above.

In the following Section we outline the experimental techniques. In Section 3 the magnetic phase transition and 2D Ising-like behavior of Fe/Pd(100) are summarized. In Section 4 the surface magnetic anisotropy of Fe ultrathin films is surveyed. Ferromagnetic *dead* layers of Fe/Ru(0001) are discussed in Section 5 . The final Section consists of a summary.

2. EXPERIMENTAL BACKGROUND

To prepare the samples, mechanically or electrochemically polished substrates were cleaned in 10^{-11} Torr ultrahigh vacuum (UHV) using repeated Ar^+ sputter and anneal cycles. Homoepitaxial evaporation of substrate materials was used to smooth the surface. Low-energy electron diffraction (LEED) was used to verify the epitaxial growth; Auger electron spectroscopy was used to study the growth mode, the cleanness, and the thickness of the films. As an example, Fig. 1 shows Auger intensity-*vs* -deposition-time curves for Fe grown on Pd(100) at 300 K. The data can be fitted to exponential curves [Fig. 1(a)] and can also be fitted as straight-line segments with two equally-spaced breaks. The breaks indicate the completion of the first and second monolayers. The inelastic

mean-free-path parameters thus deduced (5.8 Å for the Pd 330-eV and 9.4 Å for the Fe 654-eV Auger electrons) are close to the values that appear in the universal curve [25]. These results are indicative of a predominantly layer-by-layer growth mode. The same LEED-Auger procedure has been repeated for the films grown at 100 K. The main differences appear as broadened LEED spots and a faster substrate Auger signal decay compared to the 300-K growth results.

In-situ surface magneto-optic Kerr effect (SMOKE) measurements were used to detect the magnetization and the easy axes of the films. A pair of crossed electromagnets inside the UHV chamber provides a magnetic field either perpendicular or parallel to the film plane for the polar or longitudinal Kerr-effect configuration, respectively. A p-polarized He-Ne laser is reflected from the film and detected by a crystal prism polarizer and a silicon photodiode. Reversing the direction of the magnetization reverses the polarization state of the reflected light and changes the intensity at the detector. A hysteresis loop is then generated when the field is swept along the easy axis of the film. The hysteresis height, referred to as the Kerr intensity, represents the change of polarization and is proportional to the film magnetization [26, 27]. A polar Kerr-effect hysteresis loop with remanence serves as direct evidence of the presence of perpendicular magnetic anisotropy. For instance, Fig. 2 shows SMOKE loops for 1-, 2-, and 3-ML films of Fe/Pd(100) grown and measured at room temperature. Under this growth condition, the easy axis of magnetization is in the film plane, as shown by the presence of longitudinal Kerr-effect hysteresis loops and the absence of polar loops. When the film is grown at lower substrate temperatures (below ~270 K), the easy axis is out-of-plane in the monolayer region and polar square loops are observed. Figure 3 shows the SMOKE signals for Fe/Pd(100) grown and measured at ~100 K. The presence of submonolayer ferromagnetism and the reorientation of the easy axis from vertical to in-plane with increasing film thickness are apparent.

3. MAGNETIC PHASE TRANSITION AND CRITICAL BEHAVIOR OF Fe/Pd(100)

SMOKE is also used to study the temperature dependence of the magnetization and, hence, the magnetic phase transition. The temperature dependence of the Kerr intensity can be obtained either from individual hysteresis loops, as shown in Fig. 4(a) for longitudinal measurements, or by directly recording only the height of the loop in the remanent state, as shown in Fig. 4(b) for polar measurements. From Fig. 4 it is evident that all films undergo second-order phase transitions with thickness-dependent T_C values. The thermal reversibility of Fe/Pd(100) in the monolayer and submonolayer region (evidenced by the overlap of the warming and cooling data sets) is in sharp contrast to the monolayer behavior of Fe/Cu(100) [20] and Fe/Au(100)[22], and is attributed to the high surface free energy of Pd as compared to that of Cu and Au [28, 29].

The effective exponents β_{eff} deduced from Fig. 4 are all close to the 2D Ising result of $\beta_c = 1/8$. The β_{eff} values are obtained by plotting the data on a log M *vs* log(1 - T/T_C) scale using T_C as a parameter to maximize the range of a straight-line fit [30]. Figure 5 shows such log-log plots for the indicated data, which are vertically shifted for clarity. The 1.2-ML data set yields $\beta_{eff} = 0.127 \pm 0.004$, which is extremely close to the Ising value. All β_{eff} values fall between 0.13 and 0.16.

The trend in the β_{eff} values (Fig. 5) is consistent with Monte-Carlo calculations for finite-size Ising square lattices [31]. The rounding (or tails) in the transitions shown in Fig. 4 are also attributed to finite-size effects. Two boundary conditions are considered in Ref. 31, periodic and free edges. Both conditions can yield pronounced tails extending above T_C when the lateral dimensions are finite. In the calculations [31] the magnetization below T_C is relatively unaffected by periodic boundary conditions, but is lowered for free-edges. This lowering yields the trend to the larger β_{eff} values observed experimentally. Thus, the free-edge boundary conditions may provide a suitable description of the submonolayer regime.

The T_C-*vs*-thickness dependence is also consistent with the results of the Monte-Carlo calculations for Ising films [8]. Figure 6 shows the thickness-dependence of T_C as determined from the log-log-plot fitting procedure. The Monte-Carlo results, scaled to the 3-ML experimental point, are shown as small crosses and are connected by a dashed line. The agreement with the experimental data is remarkable. Figure 6 also shows the T_C-*vs*-thickness dependence in the submonolayer regime, which has not yet been the subject of theoretical treatment.

Note that the T_C thickness dependence is independent of the spin orientation of the sample. Samples grown at 100 K have vertical easy axes and are measured in the polar Kerr-effect configuration. Their T_C-values are plotted in Fig. 6 as square symbols. Samples grown at 300 K have in-plane easy axes. Their T_C-values are measured in the longitudinal configuration and plotted as triangles. Both square and triangle symbols fall on a smooth curve in Fig. 6. The square symbols are limited to being below 2 ML because of the reorientation of easy axis due to the surface magnetic anisotropy.

4. SURFACE MAGNETIC ANISOTROPY

Using SMOKE we have established [22] that the perpendicular surface magnetic anisotropy is present in ultrathin Fe films with various epitaxial structures: face-centered-cubic (fcc) Fe(100) on Cu(100), body-centered cubic (bcc) Fe(100) on Au(100), body-centered-tetragonal (bct) Fe(100) on Pd(100), and trigonally compressed Fe(111) layers on Ru(0001). For each system there exists a critical thickness d_c below which the easy axis of magnetization is perpendicular to the film and beyond which the easy axis reorients in-plane. The SMOKE results for these systems are summarized in Fig. 7. The Kerr intensity and coercivity values at various thicknesses are obtained from hysteresis loops such as the ones shown in Fig. 3. The Fe/Cu(100), Fe/Au(100), and Fe/Pd(100) data are for films grown and measured at ~100 K, while the Fe/Ru(0001) data are for films grown and measured at ~300 K.

The appearance of a critical thickness d_c is a direct evidence of perpendicular surface magnetic anisotropy. Fe/Pd(100) films less than ~2-ML thick and grown at 100 K have vertical easy axes that persist up to T_C without reorienting, while those between ~2 and ~2.6-ML thick have vertical easy axes that reorient in-plane as the temperature increases before reaching T_C.

For Fe/Au(100), previous reports [12, 24] failed to show perpendicular easy axes. We found that it is necessary to grow Fe at ~100 K on a freshly prepared Au(100) surface to obtain the desired vertical orientations (see Fig. 7). Even under these conditions the perpendicular state of Fe/Au(100) is not stable; the easy axis always reorients in-plane as temperature increases and cannot be recovered on cooling back to 100 K [22]. This is attributed to intermixing between Fe and Au.

5. FERROMAGNETIC *DEAD* LAYERS OF Fe/Ru(0001)

In Fig. 7, a striking feature of Fe/Ru(0001) is that the extrapolation to zero intensity of the Kerr-intensity curves does not go through zero thickness. Both polar and longitudinal curves extrapolate to ~2-ML. The trend in coercivity values for Fe/Ru(0001) is also significantly different than that of the other systems. Apparently, the first two monolayers of Fe/Ru(0001) are ferromagnetically *dead*. Typical SMOKE signals for Fe/Ru(0001) grown and measured at ~300 K are shown in Fig. 8 at thicknesses as indicated. The SMOKE measurements for Fe/Ru(0001) were extended down in temperature to ~30 K, without noting the appearance of ferromagnetic hysteresis for samples grown at both ~100 K and ~300 K. Similar observations have also recently been reported for Fe/Ru superlattices where no ferromagnetism was found for <4-ML of Fe (2-ML Fe on each side of Ru) [32]. Also, a recent total-energy calculation [33] for a 1-ML-Fe(111)/5-ML-Ru(0001)/1-ML-Fe(111) slab shows that the antiferromagnetic state has the lowest energy. The Kerr signals shown in Fig. 8 for the 1-ML and 2-ML films have no hysteresis, but are noticeably curved, unlike that for the pure Ru(0001) substrate. The symmetric curvature with respect to the applied field may represent the quadratic magnetic rotation such as have been observed in magneto-

optics for antiferromagnetic materials, *e.g.* FeF_2 and CoF_2 [34]. Our results will be extended to higher fields in the future to explore this issue further.

The antiferromagnetic configuration [35] is predicted to be the most favorable one for V, Cr, and Mn overlayers on the (100) surfaces of noble metals, including Pd and Pt. Fcc Fe also has ferromagnetic and antiferromagnetic states. It is well known that in dilute alloys Fe atoms lose their magnetic moment in a Ru host, due to d-band hybridization [15]. The d-band hybridization across the interface must also determine the magnetic properties of the Fe/Ru(0001) system.

6. SUMMARY

We have surveyed SMOKE studies of the magnetic properties of epitaxial Fe ultrathin films on Pd(100), Cu(100), Au(100), and Ru(0001) substrates. The unique properties of Fe/Pd(100) have made it possible to study 2D magnetic phase transitions even for submonolayer film thicknesses. The study of Fe/Pd(100) conforms to theoretical expectations that 2D Heisenberg systems with anisotropy have 2D Ising-like transitions. The effective magnetization exponent β_{eff} is found to be 0.127 ± 0.004 for a 1.2-ML Fe/Pd(100) film. Both the finite-size effect and the T_C trend with thickness are also in agreement with Monte-Carlo calculations for 2D Ising lattices.

SMOKE has also been used to detect perpendicular surface magnetic anisotropy. All of the four systems studied exhibit perpendicular spin orientations in the thickness range of a few monolayers and transform to in-plane orientations at a critical thickness d_c. The complexities of intermixing and electronic hybridization between the overlayer and substrate have been discussed. Intermixing may cause the disappearance of perpendicular spin orientations. Electronic hybridization has similar effects for Fe overlayers as for Fe in dilute alloys. The giant magnetic moment for Fe in Pd alloys may relate to the ferromagnetic response for submonolayer Fe/Pd(100) films. The missing magnetic moment for Fe in a Ru host may also relate to the lack of ferromagnetic response for the

first two Fe layers on Ru(0001). This correlation between interfaces and dilute alloys would be very valuable to pursue in future studies on monolayer magnetism.

ACKNOWLEDGMENTS

This work was supported by the U. S. Department of Energy, BES-Materials Sciences, under Contract #W-31-109-ENG-38. We acknowledge discussions with M. B. Brodsky, A. J. Freeman, K. Strandburg, and J. Zak and the technical assistance of J. Pearson.

REFERENCES

1. L. Onsager, Phys. Rev. **65** (1944) 117.
2. B. Kaufman and L. Onsager, Phys. Rev. **76** (1949) 1244.
3. C. N. Yang, Phys. Rev. **85** (1952) 808.
4. N. D. Mermin and H. Wagner, Phys. Rev. Lett. **17** (1966) 1133.
5. M. E. Fisher, Rev. Mod. Phys. **46** (1974) 597.
6. F. Y. Wu, Rev. Mod. Phys. **54** (1982) 235.
7. H. J. Mikeska, Z. Physik, **261** (1973) 437.
8. K. Binder and P. C. Hohenberg, IEEE Trans. on Magnetics, **MAG-12** (1976) 66 .
9. S. Schwarzl and H. Hoffmann, Physica, **86-88B** (1977) 1406.
10. R. M. Suter and C. Hohenemser, J. Appl. Phys. **50** (1979) 1814.
11. K. Binder and P. C. Hohenberg, Phys. Rev. **B6** (1972) 3461; **B9** (1974) 2194.
12. W. Dürr, M. Taborelli, O. Paul, R. Germar, W. Gudat, D. Pescia and M. Landolt, Phys. Rev. Lett. **62** (1989) 206 .
13. C. A. Ballentine, R. L. Fink, J. Araya-Pochet, and J. L. Erskine, Phys. Rev. **B41** (1990) 2631.
14. C. Rau, G. Xing, and M. Robert, J. Vac. Sci. Technol. A **6** (1988) 579.
15. A. M. Clogston, B. T. Matthias, M. Peter, H. J. Williams, E. Corenzwit, and R. C. Sherwood, Phys. Rev. **125** (1962) 541 .
16. D. C. Mattis, "The Theory of Magnetism I" (Springer-Verlag, Berlin, corrected 2nd printing 1988), p. 35.
17. S. Blügel, M. Weinert, and P. H. Dederichs, in Proceedings of the 18th Annual International Symposium on Electronic Structure of Solids, ed. P. Ziesche (TU Dresden, 1988), p. 101.
18. J. G. Gay and R. Richter, Phys. Rev. Lett. **56** (1986) 2728.

19. B. T. Jonker, K.-H. Walker, E. Kisker, G. A. Prinz, and C. Carbone, Phys. Rev. Lett. **57** (1986) 142.

20. C. Liu, E. R. Moog, and S. D. Bader, Phys. Rev. Lett. **60** (1988) 2422.

21. C. Liu, E. R. Moog, and S. D. Bader, J. Appl. Phys. **64** (1988) 5325.

22. C. Liu and S. D. Bader, J. Vac. Sci. Tech. A (1990), in press.

23. C. Liu and S. D. Bader, Phys. Rev. **B41** (1990) 553.

24. E. R. Moog and S. D. Bader, Superlatt. Microstruct. **1** (1985) 543.

25. C. J. Powell, Surf. Sci. **44** (1974) 29.

26. P. N. Argyres, Phys. Rev. **97** (1955) 334.

27. For recent calculations on the Kerr effect, see J. Zak, E. R. Moog, C. Liu, and S. D. Bader, J. Magn. Magn. Mater. (1990), in press.

28. A. R. Miedema, Z. Metallkde, **69** (1978) 287.

29. J. C. Hamilton, Phys. Rev. Lett. **42** (1979) 989.

30. D. L. Connelly, J. S. Loomis, and D. E. Mapother, Phys. Rev. **B3** (1971) 924 .

31. D. P. Landau, Phys. Rev. **B13** (1976) 2997.

32. M. Maurer, J. C. Ousset, M. F. Ravet, and M. Piecuch, Europhys. Lett. **9** (1989) 803.

33. Ruqian Wu and A. J. Freeman, private communication.

34. N. F. Kharchenko, A. V. Bibik, and V. V. Eremenko, JETP Lett. **42** (1985) 553.

35. S. Blügel, M. Weinert, and P. H. Dederichs, Phys. Rev. Lett. **60** (1988) 1077.

FIGURE CAPTIONS

Fig. 1. Auger intensity *vs.* deposition-time measurements for Fe grown on Pd(100) at room temperature: (a) shows the exponential least-squares fit of the data, and (b) shows linearized regions for the same data as in (a).

Fig. 2. Longitudinal (a) and polar (b) Kerr-effect signals for Fe/Pd(100) films grown and measured at ~300 K. No polar hysteresis loops were observed at any Fe thickness for films grown at ~300 K.

Fig. 3. Polar (a) and longitudinal (b) Kerr-effect signals for Fe/Pd(100) films grown and measured at ~100 K. The longitudinal Kerr-effect hysteresis loop appears when the Fe film thickness is increased.

Fig. 4. Temperature dependence of the normalized Kerr intensity for Fe/Pd(100) films grown at (a) ~300 and (b) ~100 K. The film thicknesses are indicated. Note the good reversibility of the warming (triangles) and cooling (circles) data sets.

Fig. 5. Log-log plots of the temperature dependence of the Kerr-intensity data for Fe/Pd(100) from Fig. 4. The data are vertically shifted for clarity. The values of the effective magnetization exponent are as indicated.

Fig. 6. Thickness dependence of T_C for in-plane (triangles) and vertical (squares) spin orientations. T_C values for films thicker than 2 ML with a vertical spin-orientation cannot be measured due to the reorientation of the easy axis of magnetization. The results of the Monte-Carlo calculations of Ref. [8] as scaled to the 3-ML experimental point are indicated by small crosses and connected by a dashed line.

Fig. 7. Thickness dependence of Kerr intensity (left panels) and coercivity (right panels) for epitaxial Fe films grown on the four indicated substrates. Note the critical thickness d_c

beyond which the magnetization reorients from perpendicular to in-plane. Squares represent polar Kerr-effect measurements, triangles longitudinal ones.

Fig. 8. Polar (a) and longitudinal (b) Kerr-effect signals for the Ru(0001) substrate and Fe/Ru(0001) films grown and measured at room temperature. The film thicknesses are indicated. Note that no hysteresis is observed for films that are ≤2-ML thick. The curvature observed in the 1- and 2-ML-thick films may be an antiferromagnetic magneto-optic response.

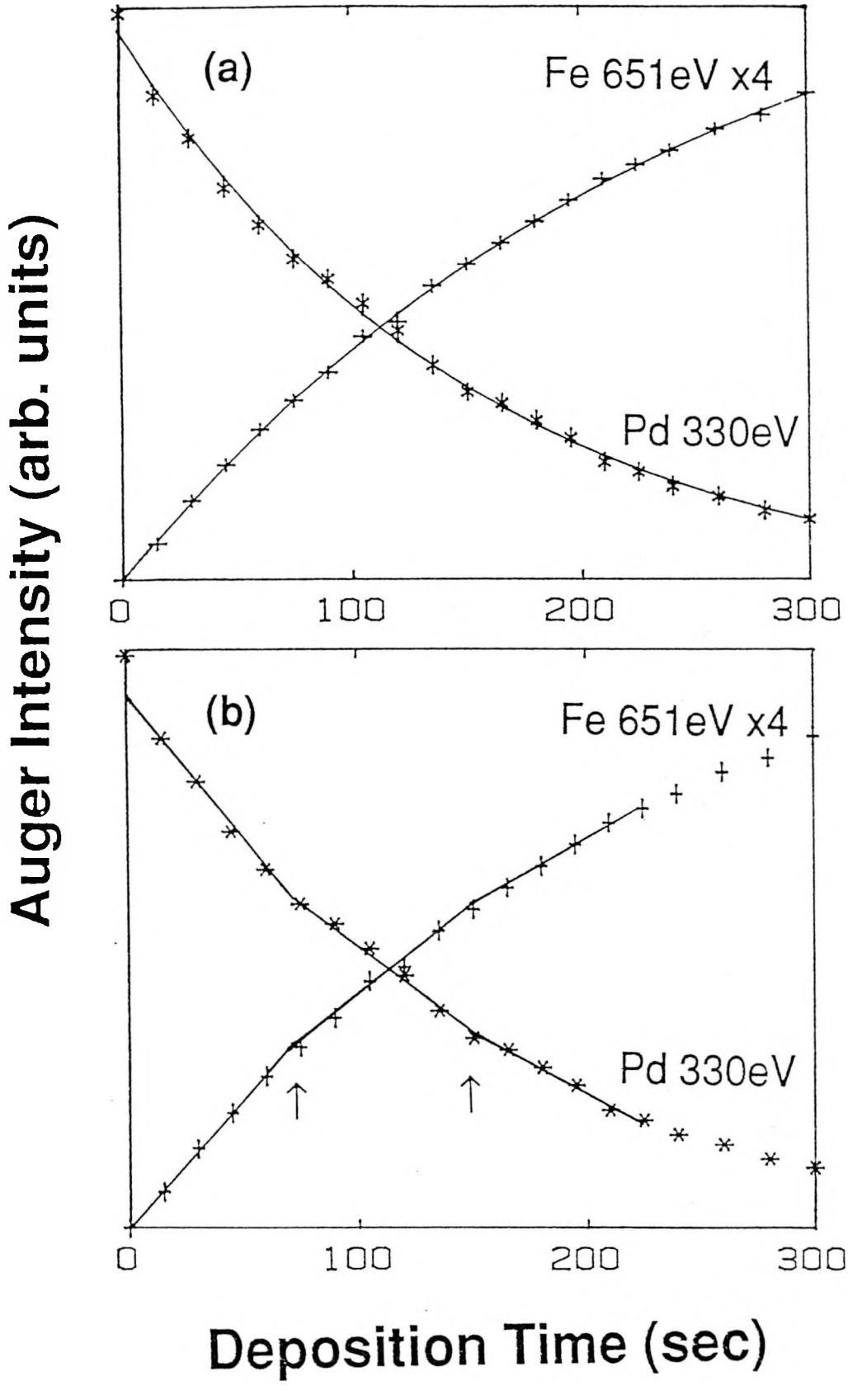
(a)
Fe 651eV x4
Pd 330eV
0
100
200
300
(b)
Fe 651eV x4
Pd 330eV
0
100
200
300
Auger Intensity (arb. units)
Deposition Time (sec)

Fig. 1

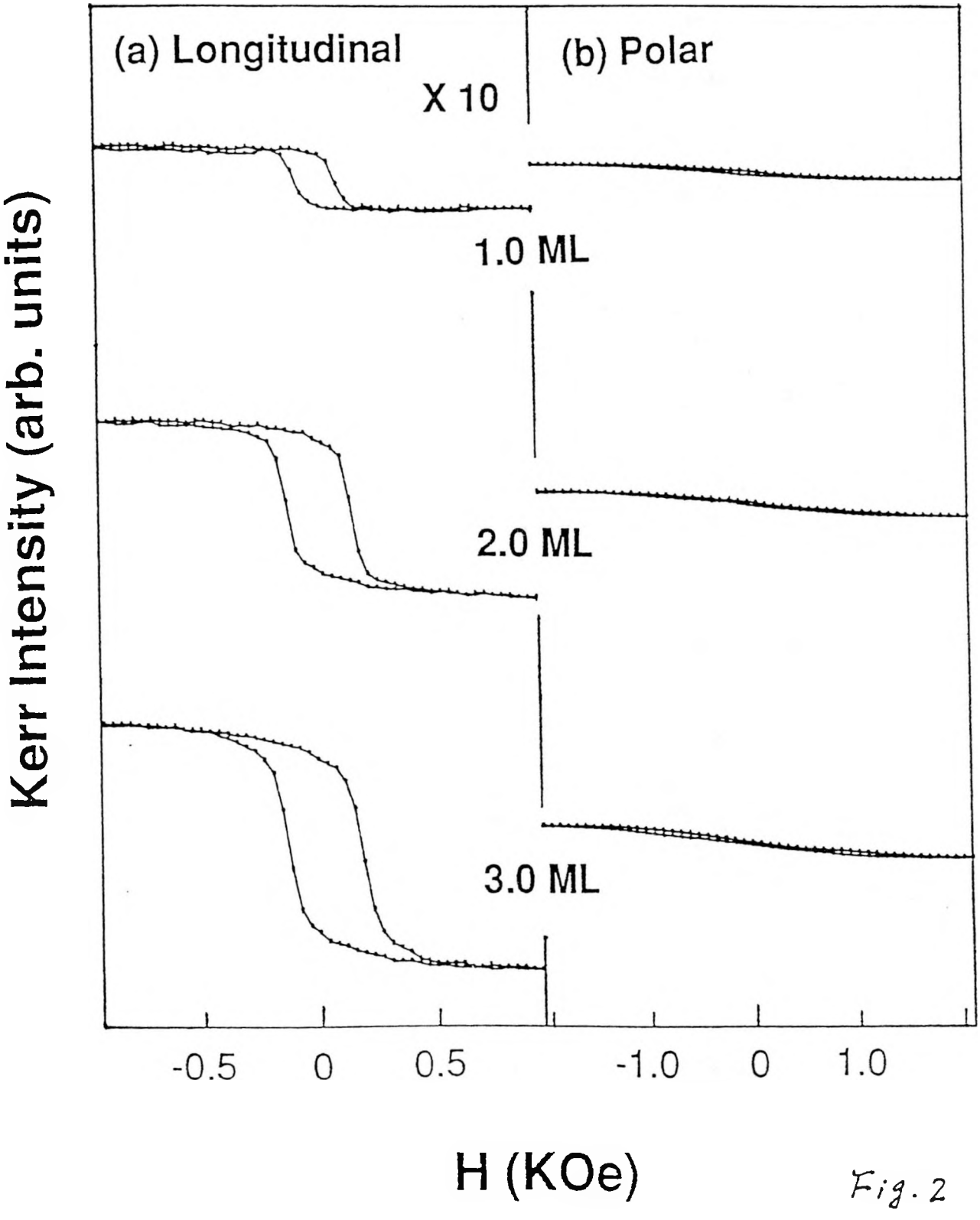
(a) Longitudinal
X 10
(b) Polar
1.0 ML
2.0 ML
3.0 ML
Kerr Intensity (arb. units)
-0.5
0
0.5
-1.0
0
1.0
H (KOe)

Fig. 2

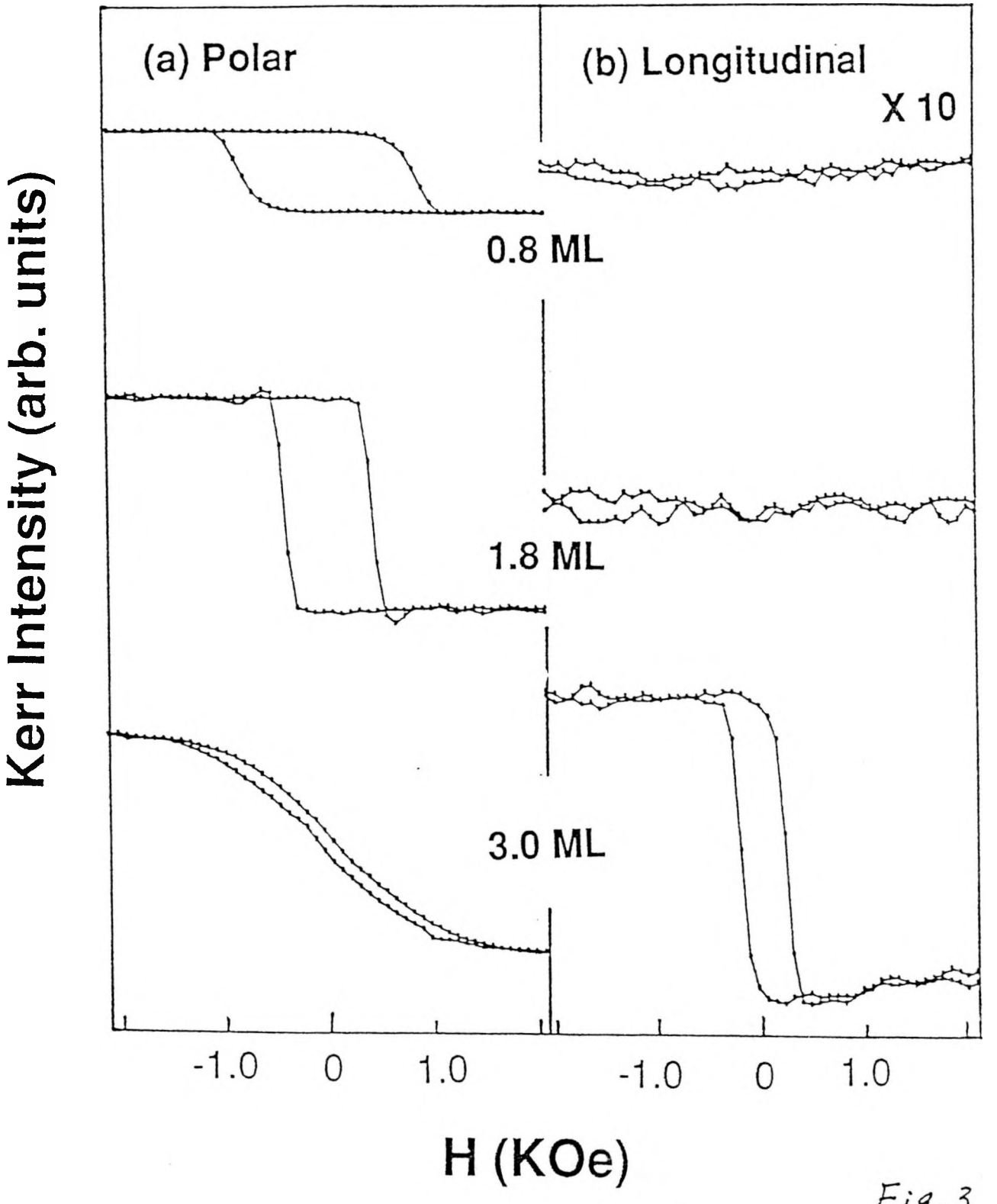
(a) Polar
(b) Longitudinal
X 10
0.8 ML
1.8 ML
3.0 ML
Kerr Intensity (arb. units)
-1.0
0
1.0
-1.0
0
1.0
H (KOe)

Fig. 3

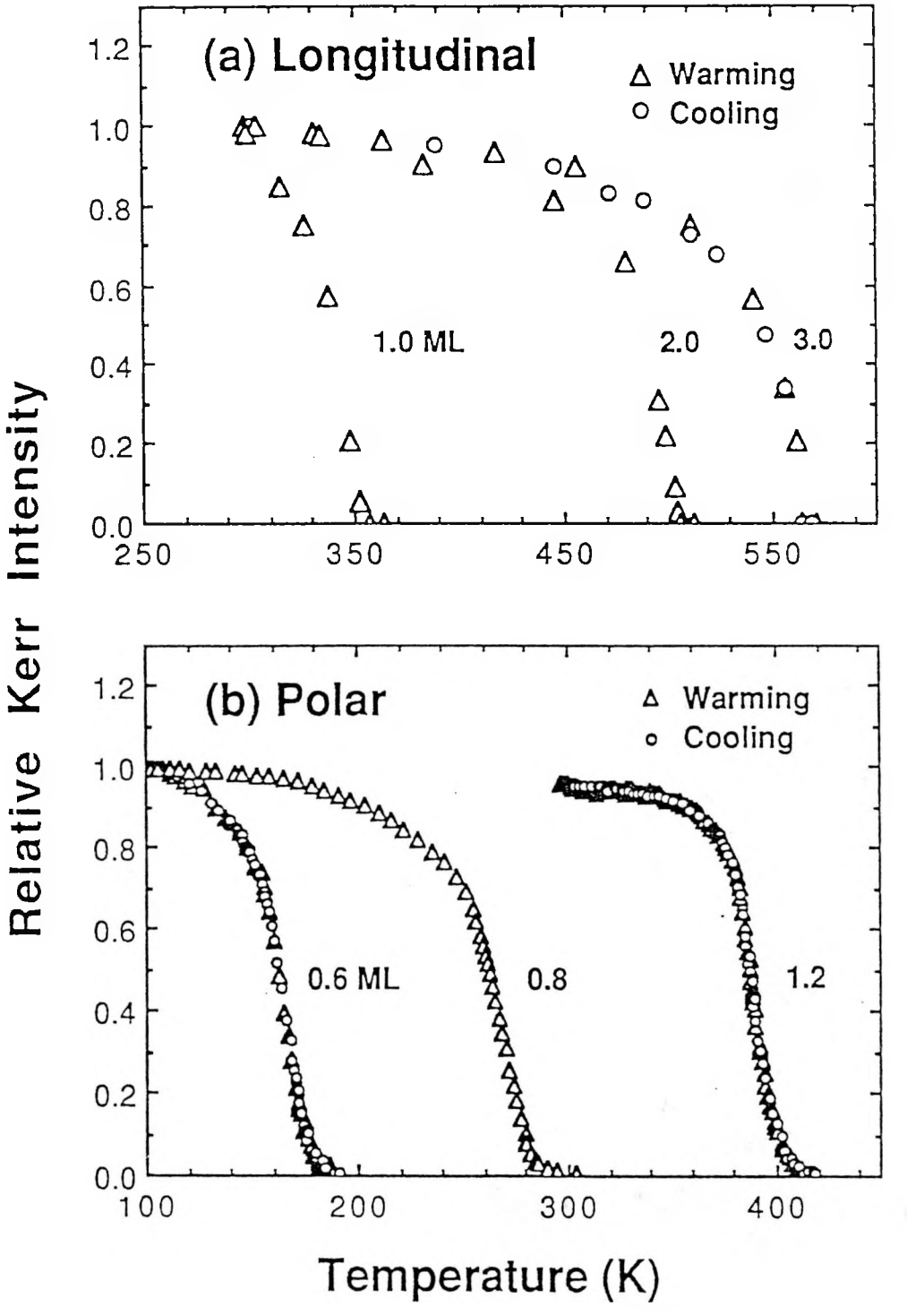
(a) Longitudinal
Warming
Cooling
1.0 ML
2.0
3.0
(b) Polar
Warming
Cooling
0.6 ML
0.8
1.2
Relative Kerr Intensity
Temperature (K)

Fig. 4

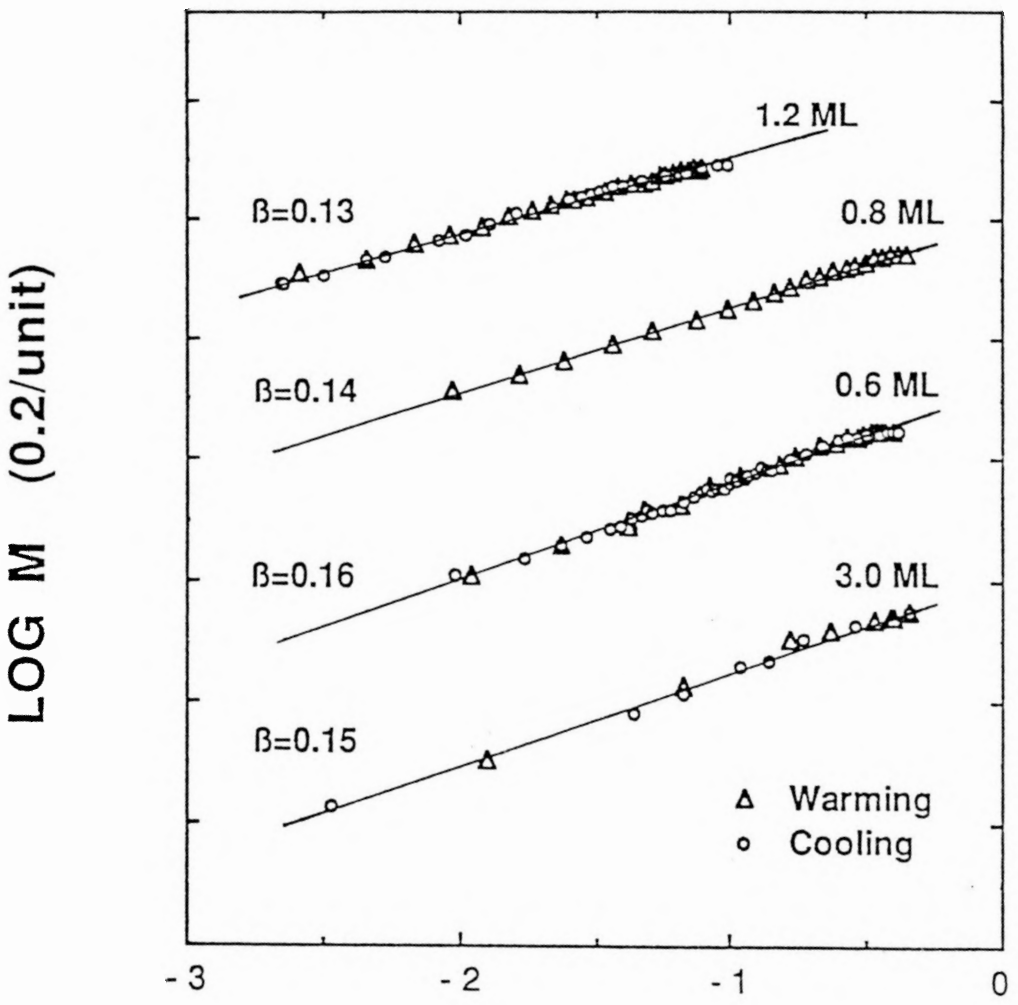
LOG M (0.2/unit)
1.2 ML
ß=0.13
0.8 ML
ß=0.14
0.6 ML
ß=0.16
3.0 ML
ß=0.15
Warming
Cooling
- 3
- 2
- 1
0
LOG(1-T/Tc)

Fig. 5

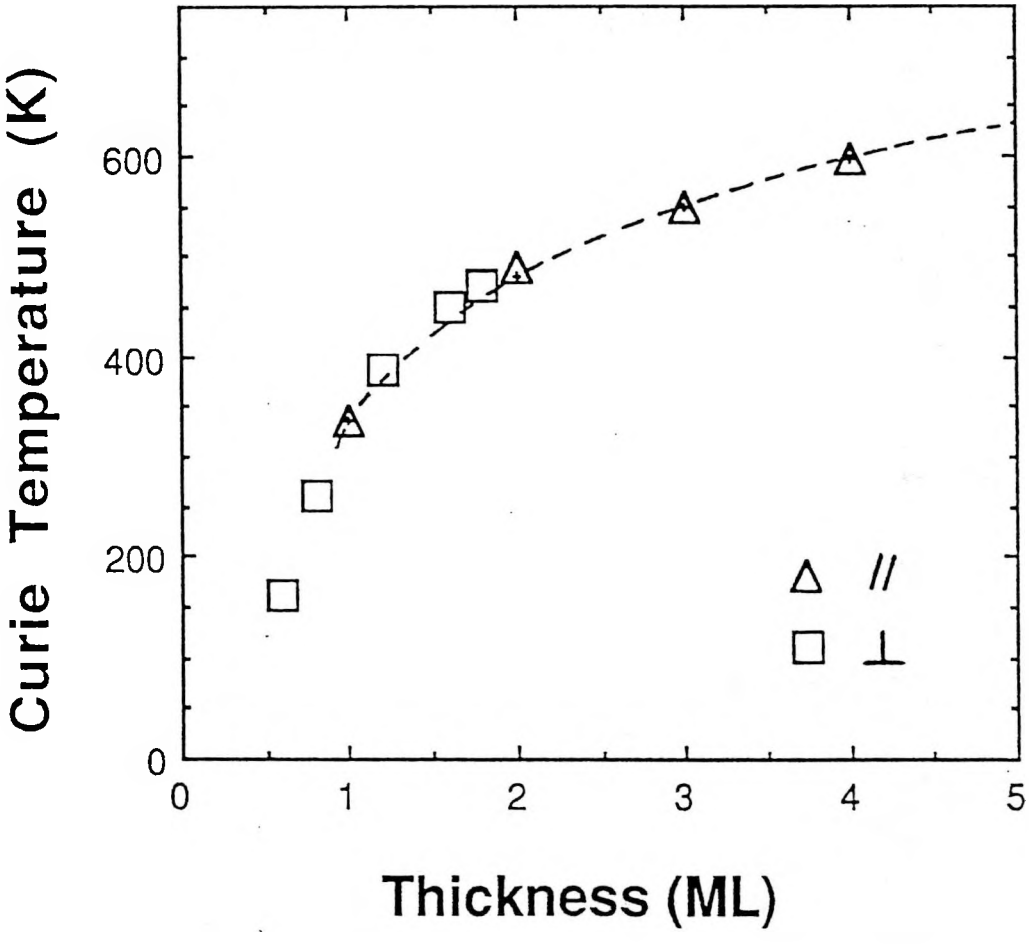

Fig. 6

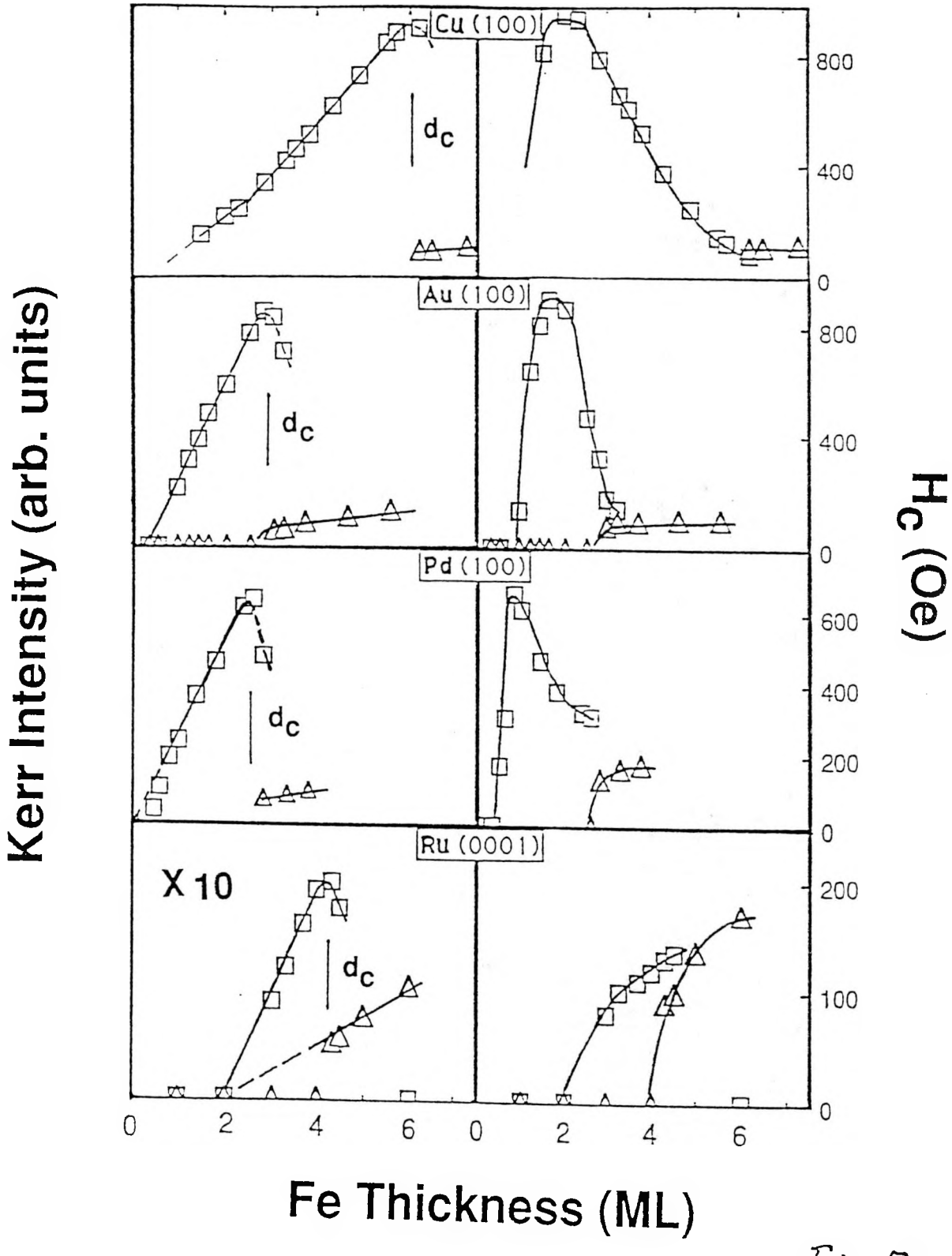
Cu (100)
Au (100)
Pd (100)
Ru (0001)
X 10
d_c
Kerr Intensity (arb. units)
H_c (Oe)
Fe Thickness (ML)
0
2
4
6
800
400
600
200
100

Fig. 7

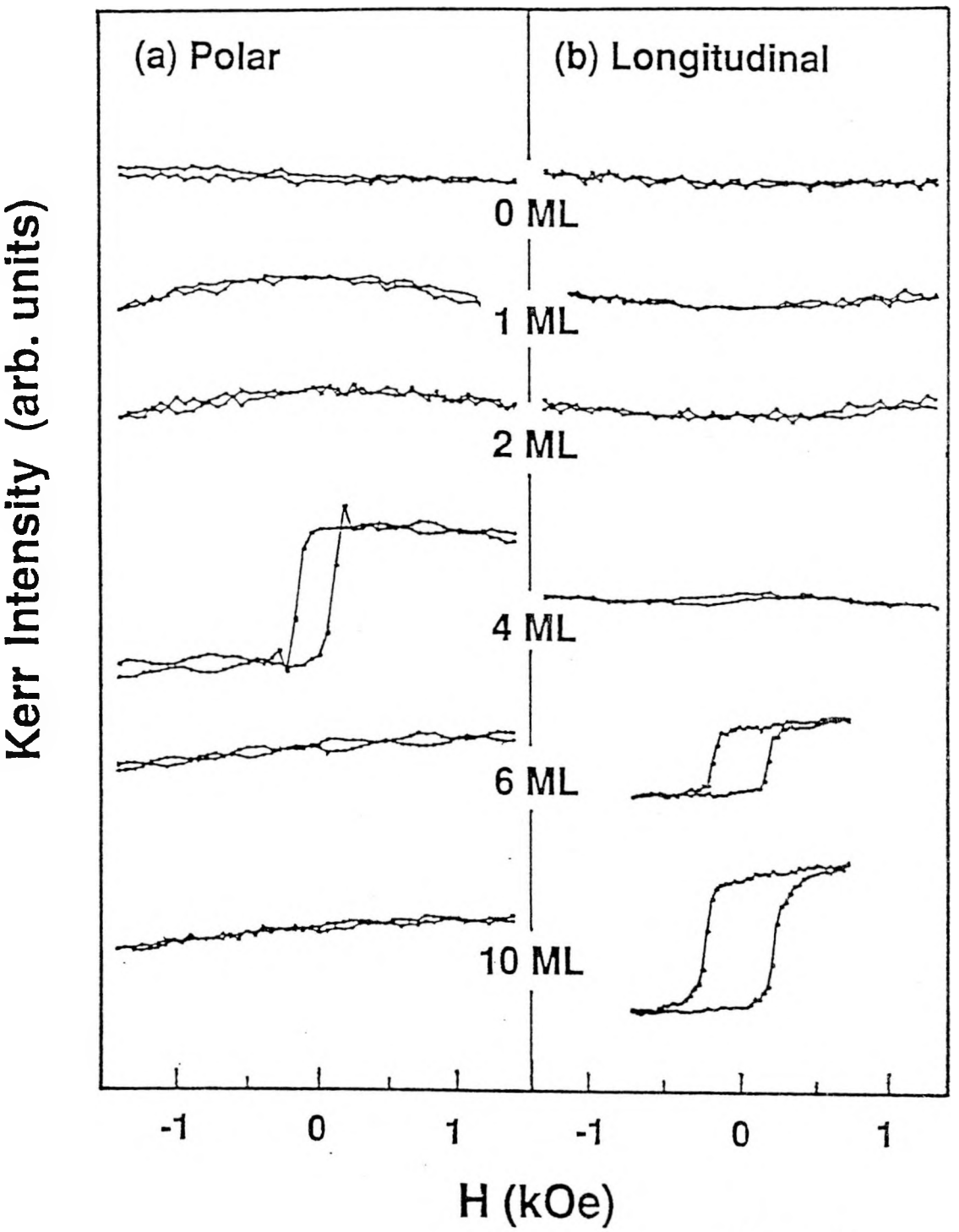
(a) Polar
(b) Longitudinal
0 ML
1 ML
2 ML
4 ML
6 ML
10 ML
Kerr Intensity (arb. units)
-1
0
1
-1
0
1
H (kOe)

Fig. 8